© 2017. Published by The Company of Biologists Ltd | Journal of Experimental Biology (2017) 220, 3419-3431 doi:10.1242/jeb.161125

RESEARCH ARTICLE

Turbulence induces metabolically costly behaviors and inhibits food capture in oyster larvae, causing net energy loss

Heidi L. Fuchs‡, Jaclyn A. Specht, Diane K. Adams and Adam J. Christman*

ABSTRACT

Planktotrophic invertebrate larvae require energy to develop, disperse and settle successfully, and it is unknown how their energetics are impacted by turbulence. Ciliated larvae gain metabolic energy from their phytoplankton food to offset the energetic costs of growth, development and ciliary activity for swimming and feeding. Turbulence may affect the energetic balance by inducing behaviors that alter the metabolic costs and efficiency of swimming, by raising the encounter rate with food particles and by inhibiting food capture. We used experiments and an empirical model to quantify the net rate of energy gain, swimming efficiency and food capture efficiency for eyed oyster larvae (*Crassostrea virginica*) in turbulence. At dissipation rates representative of coastal waters, larvae lost energy even when food concentrations were very high. Both feeding activity and turbulence-induced behaviors incurred high metabolic costs. Swimming efficiency was concave up versus dissipation rate, suggesting that ciliary activity for food handling became more costly while swimming became more efficient with turbulence intensity. Though counter-intuitive, swimming may have become more efficient in turbulence because vorticity-induced rotation caused larvae to swim more horizontally, which requires less effort than swimming vertically against the pull of gravity. Overall, however, larvae failed to offset high activity costs with food energy gains because turbulence reduced food capture efficiency more than it enhanced food encounter rates. Younger, smaller larvae may have some energetic advantages, but competent larvae would lose energy at turbulence intensities they experience frequently, suggesting that turbulence-induced starvation may account for much of oysters' high larval mortality.

KEY WORDS: Aerobic scope, Capture efficiency, Ciliary swimming, Clearance rate, Kolmogorov scale, Swimming efficiency

INTRODUCTION

Most benthic populations depend on a supply of planktonic larvae, but nearly all larvae die during the dispersal phase (typically >99.9%; Thorson, 1950), and it remains unknown how larval energetics or survival varies with environmental conditions such as turbulence. Planktotrophic larvae expend metabolic energy to grow, develop and swim, while gaining energy from feeding on phytoplankton. Metabolic gains must balance or exceed metabolic costs for larvae to maintain or increase their body mass. Energetic relationships in turbulence have been described for fish and crustaceans (e.g. Alcaraz, 1997; Galbraith et al., 2004) but may differ in weakly swimming, ciliated larvae that both swim and feed using the same appendages. Larval swimming, feeding and metabolic rates have been described separately in still water (e.g. Strathmann, 1975; Gallager, 1993; Whitehill and Moran, 2012), but it is unknown how these processes interact, and still-water studies have overlooked the effects of turbulence on swimming and suspension feeding. These gaps prevent us from relating conditions experienced during dispersal to larval growth, mortality or fitness.

Turbulence may alter energetic costs by inducing larvae to change their behavior. Turbulence produces intermittent velocity gradients that accelerate, deform or rotate the fluid around a larva (e.g. Koehl and Cooper, 2015; Pepper et al., 2015). These gradients induce some larvae to swim upward with more force (McDonald, 2012; Fuchs et al., 2015a,b), enabling them to avoid the 'gyrotactic sinking' caused by flow-induced rotation of negatively buoyant plankters (Jonsson et al., 1991; Durham et al., 2009; Clay and Grünbaum, 2010). Some mollusk larvae (veligers) also respond to turbulence by sinking or diving more frequently (Fuchs et al., 2004, 2013), a response that would concentrate larvae lower in the water column and increase settlement fluxes in turbulent coastal environments (Fuchs et al., 2007; Fuchs and Reidenbach, 2013; Hubbard and Reidenbach, 2015). Both forms of positional control carry an energetic cost, and snail and oyster larvae expend up to 100× more swimming power in strong turbulence than in still water (Fuchs et al., 2015b; H.L.F., G. P. Gerbi, A.J.C. and E. J. Hunter, unpublished data). Although ciliary swimming uses a small fraction of metabolic energy in still water (≤1%, Crawford, 1992), the added effort observed in turbulence could double the total metabolic rate if swimming efficiency remained constant. However, swimming efficiency varies with behavior, and larvae may also be able to 'buffer' their swimming efficiency by reallocating their intracellular energy use (Pan et al., 2015). Direct estimates of swimming efficiency are lacking for ciliated metazoans but are needed to assess how turbulence-induced behavior affects larval energetic costs.

Any behavioral increase in active metabolic costs must be offset with metabolic energy gained from food, but turbulence – and the behaviors it induces – may make feeding more difficult. Food encounter rates increase with the relative speed of plankters and their prey and are higher in turbulence (Rothschild and Osborn, 1988; Kiørboe and Saiz, 1995), whereas the capture efficiency may decrease with both increasing speed and turbulence intensity (Shimeta and Jumars, 1991), potentially leading to a dome-shaped relationship between turbulence and ingestion rates (MacKenzie et al., 1994). Both the positive and negative effects of turbulence on feeding could be enhanced when turbulence induces larvae to swim faster. Alternatively, feeding may stop altogether if turbulence induces larvae to sink by stopping the ciliary beat. These observed reactions to turbulence likely would cause larvae to encounter more

Department of Marine and Coastal Sciences, Rutgers, the State University of New Jersey, New Brunswick, NJ 08901, USA.
*Present address: University of Notre Dame, Notre Dame, IN 46556, USA.

‡Author for correspondence (hfuchs@marine.rutgers.edu)

H.L.F., 0000-0001-5017-2327

Received 18 April 2017; Accepted 12 July 2017

Journal of Experimental Biology (2017) 220, 3419-3431 doi:10.1242/jeb.161125

List of symbols and abbreviations

C_a	algal food concentration
COT	cost of transport
d	larval shell length
E	net rate of energy gain
E_{active}	active metabolic rate
E_{food}	rate of metabolic gain from feeding
E_{met}	total metabolic rate
E_{std}	standard metabolic rate
F	clearance rate
FAS	factorial aerobic scope
F_{max}	maximum clearance rate (=encounter rate)
$\mathbf{F}_v$	propulsive force vector
I	ingestion rate
P_o	power output
R	total respiration rate
R_{active}	active respiration rate
r_e	encounter distance (=sum of larval and algal radii)
Re_p	particle Reynolds number
R_{std}	standard respiration rate
u, w	horizontal and vertical fluid velocity
u_b, w_b	horizontal and vertical larval behavioral velocity
u_o, w_o	horizontal and vertical observed larval translational velocity
$\mathbf{V}_b$	larval behavioral velocity vector
w_T	larval terminal sinking velocity
β_b	food encounter rate due to behavior
β_t	food encounter rate due to turbulence
ε	dissipation rate of turbulent kinetic energy
η_a	food assimilation efficiency
η_k	Kolmogorov length scale
η_p	particle capture efficiency
η_s	swimming efficiency
ξ	vorticity
ϕ	angle of larval axial rotation due to vorticity

food particles but capture them less efficiently, making it more difficult to offset activity costs with food.

Turbulence may also reduce capture efficiency by interfering with larval feeding currents. Veligers use a double band of cilia to draw water towards the velum while hovering at near-zero speed, a common feeding mechanism for negatively buoyant plankton (Emlet et al., 1985; Gallager, 1993; Fenchel and Ockelmann, 2002; Kiørboe and Jiang, 2012). Particles are captured between the ciliary bands and passed along a food groove to the mouth (Strathmann and Leise, 1979; Gallager, 1988). As turbulence intensifies and the dissipation rate ε of turbulent kinetic energy increases, the smallest (Kolmogorov-scale) eddies grow smaller and can become smaller than the larvae. At the larval scale, this transition entails a shift from mostly laminar fluid motions to stronger, more spatially variable velocity gradients that could erode larval feeding currents (Lazier and Mann, 1989; Marrasé et al., 1990; Sutherland et al., 2014). Larvae may be able to offset this effect by producing stronger feeding currents, but doing so probably carries added energetic costs. Kolmogorov-scale erosion of feeding currents could reduce particle capture efficiency, potentially handicapping the larval ability to gain energy in strong turbulence.

We investigated how turbulence affects energetics of larval oysters, *Crassostrea virginica* Gmelin 1791. In turbulence, oyster larvae react primarily to fluid rotation (vorticity), sensed using simple gravity-detecting organs (statocysts; Fuchs et al., 2015a). Turbulence induces oyster larvae to swim more strongly upward and to dive downward with greater frequency and effort (Wheeler et al., 2013; Fuchs et al., 2013, 2015a,b). These flow-induced behaviors will raise the metabolic cost of swimming, but by how much depends on the unknown swimming efficiency. Both turbulence and flow-induced faster swimming would enable larvae to encounter more food but might make its capture more difficult. Although there is a theoretical basis for estimating encounter rates in turbulence (Shimeta and Jumars, 1991; Kiørboe and Saiz, 1995), the effects of turbulence on particle capture efficiency are less well characterized for ciliary swimmers, and it is unknown how food capture is affected by the relative sizes of larvae and eddy motions. The goal of these laboratory experiments was to simultaneously quantify how turbulence affects the net rate of energy gain, swimming efficiency and particle capture efficiency to better understand hydrodynamic control of larval energy acquisition.

Energetic theory

The net rate of larval metabolic energy gain or loss $E(t)$ over time t is:

$$E(t) = -E_{met} + E_{food}, \quad (1)$$

where E_{met} is the total metabolic cost and E_{food} is the rate of energy gain due to feeding (e.g. Tucker, 1975; Visser et al., 2009). Metabolic costs are a sum of standard and active metabolism:

$$E_{met} = E_{std} + E_{active}, \quad (2)$$

where E_{std} includes body maintenance and larval development (e.g. Clarke and Fraser, 2004), and E_{active} is the cost of ciliary activity for swimming and feeding. This basic model can be used to estimate larval fitness or growth rate (Gerritson, 1984; Visser et al., 2009). For larvae, standard metabolism (E_{std}) is roughly proportional to body mass (e.g. Zeuthen, 1953; Hoegh-Guldberg and Manahan, 1995). In contrast, the activity costs (E_{active}) and feeding benefits (E_{food}) will vary with behavior, turbulence and food concentration.

The cost of swimming (E_{active}) generally increases with body size and speed and decreases as swimming becomes more efficient (Lighthill, 1952; Tucker, 1975; Morris et al., 1985; Visser et al., 2009). The net swimming efficiency:

$$\eta_s = P_o / E_{active}, \quad (3)$$

relates activity costs to power output P_o, or useful work done to the surrounding fluid via swimming (=speed×magnitude of propulsive force). Swimming efficiency is a ratio of mechanical work of moving the larvae to metabolic work required to swim, and can be derived as a product of ciliary work efficiency and the mechanical efficiency of moving through the water (Morris et al., 1985; Crawford, 1992). The mechanical efficiency, and thus η_s, varies with the particle Reynolds number, defined here as $Re_p = d|\mathbf{V}_b|/\nu$, where d is larval length, $\mathbf{V}_b$ is the larval velocity relative to the water, vertical bars indicate vector magnitude and ν is kinematic viscosity.

Swimming efficiency is well studied for neutrally buoyant organisms at low particle Reynolds numbers (e.g. Sleigh and Blake, 1977; Katsu-Kimura et al., 2009; Osterman and Vilfan, 2011), where most of the metabolic energy expended in swimming is used to overcome viscous drag (e.g. Lighthill, 1952). Under these conditions, efficiencies for ciliary swimmers are often $\eta_s \leq 1.0\%$ (Crawford, 1992). However, negatively buoyant veligers can experience net gravitational forces greatly exceeding the drag forces (Fuchs et al., 2015b), and efficiency should vary as larvae swim upward – against gravity – or downward – with gravity. Many larvae also reach intermediate particle Reynolds numbers ($Re_p \leq 10$) where form drag and Basset history forces become non-negligible (Maxey and Riley, 1983; Mei et al., 1991; Guseva et al., 2013; Fuchs et al., 2015b), further reducing swimming efficiency.

Journal of Experimental Biology (2017) 220, 3419-3431 doi:10.1242/jeb.161125

Veligers should have lower swimming efficiency and higher activity costs when ascending than when descending, and activity costs may vary nonlinearly with speed as larvae transition from $Re_p<1$ to $Re_p>1$.

For larvae to survive and grow, metabolic costs must be balanced or exceeded by energy gained from food:

$$E_{food} = eI\eta_a, \quad (4)$$

where e is energy per food particle, I is ingestion rate and η_a is assimilation efficiency (e.g. Visser et al., 2009). Ingestion rate is:

$$I = C_a F, \quad (5)$$

where C_a is algal concentration and F is filtration or clearance rate. Ingestion rates could vary with turbulence intensity as water motion alters the encounter rate with food particles and the efficiency of food capture. We quantify these effects by defining clearance rate as:

$$F = F_{max}\eta_p, \quad (6)$$

where F_{max} is the maximum clearance rate, equivalent to encounter rate if all encountered food particles are captured, and η_p is the particle capture efficiency. The maximum clearance rate F_{max} is:

$$F_{max} = \beta_b + \beta_t, \quad (7)$$

where β_b is volumetric encounter rate due to larval behavior and β_t is the volumetric encounter rate due to turbulence (Kiørboe and Saiz, 1995). We assume that larvae swim steadily and algae are immobile, so:

$$\beta_b = \pi r_e^2 V_b, \quad (8)$$

where r_e is the encounter distance or sum of the larval and algal radii. The encounter rate due to turbulence depends on larval length d relative to the smallest eddy length:

$$\beta_t = \begin{cases} 0.42\pi r_e^3 \left(\frac{\varepsilon}{\nu}\right)^{0.5} & \text{if } d < \eta_k \\ 1.37\pi\varepsilon^{1/3} r_e^{7/3} & \text{if } d > \eta_k \end{cases}, \quad (9)$$

(Kiørboe and Saiz, 1995) where $\eta_k=(\nu^3/\varepsilon)^{0.25}$ is the Kolmogorov length scale, ν is the kinematic viscosity and ε is the dissipation rate of turbulent kinetic energy. Hereafter we refer to the dissipation rate where $\eta_k=d$ as the $\varepsilon|_{\eta_k=d}$ threshold, which defines a shift in the dependence of encounter rate on turbulence.

MATERIALS AND METHODS

Eyed oyster (*C. virginica*) pediveligers were obtained from a hatchery in June and July 2016 and were presumed to be competent (Baker, 1994). Larvae were used within 3 days of arrival, during which they were held at 20°C and 11.5 S_p (practical salinity units; matched to rearing conditions) and fed daily with live *Isochrysis galbana* (10^5 cells ml^{-1}). Experiments were performed in a temperature-controlled room at 20.5°C and 11.5 S_p and included simultaneous measurements of larval respiration, feeding and behavior. Respiration measurements require an airtight seal, so experiments were performed in 30 ml, square respirometry flasks with turbulence generated by magnetic stir bars. The bars create vortical motions with more irregularity and intermittency than the Burgers vortex used recently for studies of copepod behavior in turbulence (Jumars et al., 2009; Webster et al., 2015). Although respirometry flasks lack the large eddies of natural turbulence, larval sensory organs are much smaller than all eddy motions, so flow sensing depends only on the magnitude of velocity gradients (Fuchs and Gerbi, 2016).

Flow characterizations

We characterized fluid motions in the respirometry flasks using two-dimensional (2D), infrared (IR; 808 nm) particle image velocimetry (PIV; e.g. Adrian, 1991; Fuchs et al., 2013). The infrared laser was used during larval experiments to avoid behavioral artifacts (Fuchs et al., 2013) and was also used to characterize flow. PIV measurements were replicated at stirring frequencies of f=60, 125 and 350 rpm representing low, moderate and high turbulence intensities, respectively. After a 10 min spin-up period, flasks were observed for 3 min in a vertical image plane centered over the stir bar. Images were cropped to exclude the stirring magnet and the blurred regions at the flask corners, giving an effective image size of 1.9 cm high×4.3 cm wide that resolved 64% of the central plane inside the flask. Vector resolution was Δx=0.08 cm at the two lowest frequencies and Δx=0.04 cm at the highest frequency. Fluid velocities were computed using iterative, adaptive correlation algorithms in DynamicStudio (Dantec Dynamics, Skovlunde, Denmark), and all other calculations were performed in MATLAB (MathWorks, Natick, MA, USA). We used all observed velocity gradients to compute 2D estimates of dissipation rate:

$$\varepsilon = 3\nu\left[\overline{\left(\frac{\partial u}{\partial x}\right)^2} + \overline{\left(\frac{\partial w}{\partial z}\right)^2} + \overline{\left(\frac{\partial u}{\partial z}\right)^2} + \overline{\left(\frac{\partial w}{\partial x}\right)^2} + 2\overline{\left(\frac{\partial u}{\partial z}\frac{\partial w}{\partial x}\right)} + \frac{2}{3}\overline{\left(\frac{\partial u}{\partial x}\frac{\partial w}{\partial z}\right)}\right], \quad (10)$$

assuming that the out-of-plane gradients were of the same order as the average in-plane gradients (Doron et al., 2001; Fuchs et al., 2015b), and the vorticity $\xi = \partial w/\partial x - \partial u/\partial z$, where u and w are velocities in the horizontal x and vertical z dimensions, respectively.

Larval experiments

Larval experiments were replicated four and five times at the moderate and high turbulence levels, respectively, which had Kolmogorov scales bracketing the larval size. We were unable to complete replicates in weak turbulence because of limited availability of the respirometer. Each replicate consisted of four treatments – still water without food, still water with food, turbulence without food and turbulence with food – applied to flasks with larvae and without larvae ('blank'), for eight flasks in total. Food treatments had 10^5 cells ml^{-1} concentrated *I. galbana* (~5 µm; Reed Mariculture, Campbell, CA, USA). We used these inert cells instead of live food to avoid artifacts associated with algal respiration, swimming motion and cell division. The algal concentrations were comparable to those used to feed larval cultures and were necessarily high to enable use of algae as seeding particles for PIV observations.

Each replicate lasted 3.5 h. Four beakers were filled with larvae plus algae, larvae only, algae only and filtered seawater, and water samples were collected by pipetting through a 200 µm mesh. Beaker contents were then divided among eight respirometry flasks and distributed on two four-position digital stirrers set for still and turbulent treatments. After an initial 20-min spin-up period, oxygen measurements were collected for 30 s per flask, every half hour for 3 h and followed immediately by 5 min of PIV observations to quantify fluid motion and larval behavior in one flask; measurement details follow in subsequent paragraphs. PIV observations were made of a turbulent (+food) flask for two replicates and of a still (+food) flask for the remaining replicates at each of the two turbulence levels. After the final set of PIV observations, water

samples were pipetted through mesh for algal counts, and all larvae were collected from each flask and later counted. A separate larval sample was preserved for later measurements of shell length d and sinking velocity w_T, which were used to estimate larval density from Rubey's modification of Stokes' law (Rubey, 1933; Fuchs et al., 2013).

Respiration

Biological oxygen demand gives a proxy for metabolic rate and is typically measured using microrespirometry (Marsh and Manahan, 1999; Stumpp et al., 2011). We measured dissolved O_2 using a PreSens Fibox with fiber-optic oxygen sensors and temperature correction (e.g. Warkentin et al., 2007). The sensitivity of this instrument enabled us to keep larval concentrations relatively low, ensuring that larval collisions in turbulence were infrequent (~0.01–2 larva^{-1} h^{-1}; see Kiørboe and Saiz, 1995). Larval respiration rates R were measured and later corrected by subtracting the respiration rates measured in identically treated, larva-free blanks. The measured R includes both standard and active respiration (Eqn 2). To separate these costs, we used the respiration rates from still-water, no-food treatments as the standard respiration rates R_{std} and assumed them to be constant in other treatments for each replicate. We then estimated the active respiration rate in turbulence or food treatments as $R_{active}=R–R_{std}$. We also estimated the factorial aerobic scope:

$$\mathrm{FAS} = R/R_{\mathrm{std}}, \tag{11}$$

a useful metric of aerobic performance ability (e.g. Pörtner et al., 2010).

Feeding

Ingestion and clearance rates were calculated from the change in phytoplankton concentration in food treatments relative to larva-free, algae-only controls using a Coulter Counter (e.g. Paffenhöfer, 1971; Stumpp et al., 2011). Equations are standard (e.g. eqns 4 and 6 in Crisp et al., 1985). During the experiments, algal concentrations in the larva-free controls decreased by 22±2.8%, 15±2.0% and 19±2.6% (mean±1 s.e.m.) in the still, 125 rpm and 350 rpm treatments, respectively, indicating that there was some algal settling. Percentage decreases were not significantly different among flow treatments (one-way ANOVA, F=1.28, P=0.31). To avoid overestimation of larval ingestion and clearance rates, we calculated them relative to post-experiment concentrations in algae-only controls.

Swimming behavior

Fluid and larval motions were observed simultaneously using 2D IR PIV (e.g. Catton et al., 2007; Fuchs et al., 2013, 2015b). The IR laser limits the temporal and spatial resolution, and we were unable to resolve larval feeding currents; instead we focused on quantifying energetic mechanisms. The image field of view was 2.9 cm wide, and image heights were 100%, 25% and 12.5% of the image width at f=0, 125 and 350 rpm, respectively. Reducing the image size enabled use of higher frame rates needed for tracking individual larvae in faster flows. Because the area visualized was smaller than in flow characterizations, these images were less representative of turbulence throughout the flask and were used mainly to quantify behaviors needed for analyzing swimming efficiency and particle capture efficiency.

Fluid and larvae move in different directions, so the PIV images of particles and larvae were separated before computing velocities (two-phase flow; Kiger and Pan, 2000; Khalitov and Longmire, 2002; Fuchs et al., 2015b). Fluid velocities were computed from particle images using iterative, adaptive correlation algorithms (DynamicStudio) with vector resolutions of Δx=0.09 cm in still water and Δx=0.045 cm in turbulence. Fluid velocity gradients were used to compute 2D estimates of the instantaneous dissipation rate ε and vorticity ξ, and all physical measurements were interpolated to the positions of individual larvae (Fuchs et al., 2015b). Larval translational velocities were calculated from larval trajectories, constructed by particle tracking. The difference between these two velocities gives the larval velocity that is due to behavior, i.e. relative to flow, as a response to instantaneous local flow conditions. In the vertical (z) dimension:

$$w_{\mathrm{b}} = w - w_{\mathrm{o}}, \tag{12}$$

where w_b is the instantaneous behavioral velocity, w is the instantaneous flow velocity and w_o is the instantaneous translational (observed) velocity of an individual larva. The horizontal behavioral velocities were computed similarly for u_b in the x dimension.

Analysis

Statistics

These experiments exposed larvae to turbulence for a longer continuous interval (3.5 h) than any previous studies, so we tested for changes in behavior and turbulence over time. Using the PIV data sets collected every 30 min, we analyzed four behavior metrics (total number of larvae observed, average vertical behavioral velocity, percentage of larvae sinking or diving, and average propulsive force) and two turbulence metrics (dissipation rate and vorticity magnitude, the likely signal for changes in behavior). For each replicate, we performed linear regressions with these metrics as dependent variables and time as the independent variable. Significance was adjusted using Bonferroni corrections for multiple comparisons.

To test for interacting effects of turbulence and food, we used a two-way multivariate ANOVA (MANOVA). The independent variables were turbulence level (f=0, 125 or 350 rpm) and food (present or absent), and the dependent variables were respiration rate, ingestion rate and clearance rate. Both independent variables and their interactions had significant effects, so we also performed two-way univariate ANOVAs on respiration rate, ingestion rate and clearance rate. Significance was adjusted using a Bonferroni correction for multiple comparisons.

Energetics

Respiration and ingestion rates were used to quantify how the net rate of energy gain varied with turbulence and food availability. Respiration rates (R, R_{std} and R_{active}) were converted to metabolic rates (E_{met}, E_{std} and E_{active}) using standard oxyenthalpic equivalents (Gnaiger, 1983). Metabolic gains from feeding (E_{food}, Eqn 4) were calculated from measured ingestion rates I using an algal energy content of e=1.00×10^{-7} J cell^{-1} (Reed Mariculture) and an assimilation efficiency of η_a=0.54 (Reinfelder and Fisher, 1994). The total metabolic rate E_{met} and gains from feeding E_{food} were used in Eqn 1 to estimate the net rate of energy gain E.

We also fitted the measured respiration and ingestion rates with 2D polynomial functions of dissipation rate ε and algal concentration C_a. The initial candidate models were nested subsets of a second-order polynomial in ε and C_a (Table S1). Only models with interaction terms were considered, because MANOVA results

Journal of Experimental Biology (2017) 220, 3419-3431 doi:10.1242/jeb.161125

Table 1. Summary of flow characterizations

Level	f (rpm)	f (s^{-1})	U (m s^{-1})	W (m s^{-1})	$\overline{u'w'}$ (m^2 s^{-2})	w'_{rms}/u'_{rms}	ε (m^2 s^{-3})	η_k (cm)	σ_ξ (s^{-1})	σ^*_ξ (s^{-1})
Low	60	1.0	2.7×10^{-4}	-8.3×10^{-4}	-9.0×10^{-9}	1.15	1.4×10^{-6}	0.094	0.54	0.68
Moderate	125	2.1	2.1×10^{-3}	-3.0×10^{-3}	2.6×10^{-7}	1.07	1.5×10^{-5}	0.051	1.71	2.23
High	350	5.8	6.7×10^{-4}	-7.8×10^{-3}	-4.7×10^{-7}	0.97	2.1×10^{-4}	0.026	6.35	8.35

Values are averaged over time and space and shown as means of two replicates. Includes stirring frequency f, mean horizontal and vertical velocities U and W, Reynolds stress $\overline{u'w'}$, isotropy ratio w'_{rms}/u'_{rms}, dissipation rate ε, Kolmogorov length scale η_k, vorticity standard deviation σ_ξ, and theoretical vorticity standard deviation σ^*_ξ for isotropic turbulence with dissipation rate ε (Taylor, 1935; Fuchs and Gerbi, 2016).

indicated that turbulence–food interactions were significant. We fitted each model to the measured R or I using multiple linear regression and used the minimum Akaike information criterion with small-sample bias correction (AICc) (e.g. Burnham and Anderson, 2002) to select R^* and I^*, respectively (Table S2), where asterisks indicate model fits. A similar analysis of the Bayesian information criterion (BIC) produced identical results. The fitted R^* and I^* were converted to metabolic rates E^*_{met} and feeding gains E^*_{food} and used in Eqn 1 to predict the net rate of energy gain E^* across gradients of turbulence intensity and food concentration.

Swimming behavior and efficiency

PIV data were used to quantify swimming mechanics and power outputs of individual larvae; complete details are provided in the appendix of Fuchs et al. (2015b). The larval mass times acceleration is balanced by a vector sum of other forces, including gravity, buoyancy, drag, Basset history forces, fluid acceleration and the force that larvae exert to propel themselves (Maxey and Riley, 1983; Mei et al., 1991; Fuchs et al., 2013, 2015b). By assuming larvae to be spherical, all terms except propulsive force can be computed from measured velocities, larval size and density (Fuchs et al., 2013). We used these data to solve the force balance equation for the propulsive force vector $\mathbf{F}_v$, which indicates the magnitude and Cartesian direction of larval swimming effort. We also used the instantaneous vorticity at each larval location to calculate the angle of flow-induced larval rotation ϕ (Kessler, 1986; Fuchs et al., 2013), needed to compute the direction of propulsion relative to the body axis. We then classified larvae as swimming if they propelled themselves upward and as sinking or diving if they propelled themselves downward, relative to the body axis. Finally, the larval power output was calculated as:

$$P_o = |\mathbf{F}_v||\mathbf{V}_b|. \quad (13)$$

The PIV data enabled us to assess how total metabolic cost E_{met} was affected by turbulence through changes in swimming efficiency η_s (Eqn 3). Swimming efficiency was computed from the metabolic cost of activity E_{active}, measured as a population average for each flask, and from power output P_o, measured instantaneously for individual larvae. To relate these population- and individual-level measurements, we calculated η_s using flask-averaged values of P_o and again using regression fits to P_o (linear) and E_{active} (quadratic) versus $\log_{10}\varepsilon$. We also calculated the cost of transport (COT) for individual larvae:

$$\mathrm{COT} = \frac{E_{active}}{m\mathbf{V}_b}, \quad (14)$$

where m=2×10^{-8} kg is the average larval mass. Because E_{active} values are population averages, the estimated η_s and COT do not span the full range for individual behaviors.

Particle capture efficiency

The PIV data also enabled us to assess how the metabolic gain from food E_{food} was affected by turbulence through changes in encounter rates and particle capture efficiency (Eqn 6). For each flask observed with PIV, we computed the food encounter rate F_{max} for individual larvae using instantaneous behavioral velocities and local instantaneous dissipation rates (Eqns 7–9). To relate these individual-scale estimates to the whole-flask measurements of clearance rate F, we performed linear regressions on clearance rate (F^*) versus $\log_{10}\varepsilon$ and on encounter rate (F^*_{max}) versus ε, which better captured how encounter rates varied around the $\varepsilon|_{\eta_k=d}$ threshold. Assuming that feeding was 100% efficient in still water, we estimated particle capture efficiency as:

$$\eta^*_p(\varepsilon) = \frac{F^*(\varepsilon)}{F^*_{max}(\varepsilon) + \Delta F}, \quad (15)$$

where $\Delta F = (F^* - F^*_{max})|_{still}$ is a correction factor evaluated at the lowest mean dissipation rate observed in still-water treatments. This correction was needed because in still water, measured clearance rates exceeded the theoretical maximum, probably because larval feeding currents caused food particles to accelerate near the velum at a spatial scale too small to be resolved by our PIV measurements.

Table 2. Summary of larval measurements associated with each experimental replicate

f (rpm)	Replicate	PIV (T/S)	Concentration (larvae ml^{-1})	d (μm)	w_T (cm s^{-1})	ρ_p (g cm^{-3})
125	1	S	10.5±2.92	319±15	−0.69±0.04	1.16
125	2	T	7.33±4.66	319±11	−0.68±0.12	1.15
125	3	S	11.1±2.63	315±14	−0.74±0.11	1.17
125	4	T	4.33±1.56	321±12	−0.71±0.06	1.16
350	1	S	7.72±2.00	325±18	−0.82±0.08	1.18
350	2	T	4.83±1.51	324±14	−0.82±0.09	1.18
350	3	S	6.90±2.11	325±18	−0.78±0.15	1.17
350	4	T	5.64±2.57	315±12	−0.67±0.07	1.16
350	5	S	7.86±2.37	319±13	−0.72±0.06	1.16

Includes stirring frequency (f), replicate number, flow condition observed by particle image velocimetry (PIV) (T, turbulent; S, still), larval concentration, larval shell length (d), larval terminal sinking velocity (w_T) and estimated larval density (ρ_p). Concentrations are given as means±1 s.d. over flasks (N=4); d and w_T are given as means±1 s.d. over larvae subsampled from each replicate, with N=121–186 for d and N=35–552 for w_T.

Journal of Experimental Biology (2017) 220, 3419-3431 doi:10.1242/jeb.161125

Table 3. MANOVA and ANOVA results

A. MANOVA Source	d.f.	Wilks' λ	*F*	*P*
Turbulence	2	0.3184	7.21	**<0.0001**
Food	1	0.0811	105.73	**<0.0001**
Turbulence×food	2	0.3459	6.54	**<0.0001**
B. ANOVA Source	**d.f.**	**MS**	***F***	***P***
Respiration rate				
Turbulence	2	11,970	3.57	0.0406
Food	1	39,663	11.84	**0.0017**
Turbulence×food	2	10,888	3.25	0.0528
Ingestion rate				
Turbulence	2	2,283,553	5.10	**0.0124**
Food	1	47,659,662	106.52	**<0.0001**
Turbulence×food	2	2,283,552	5.10	**0.0124**
Clearance rate				
Turbulence	2	5.949×10^{-5}	10.70	**0.0003**
Food	1	6.381×10^{-4}	114.82	**<0.0001**
Turbulence×food	2	5.949×10^{-5}	10.70	**0.0003**

Bold *P*-values are significant. MANOVA results are significant at α=0.05. ANOVA results are significant at Bonferroni-corrected α=0.0167.

RESULTS

Flow characterizations

Stirred flasks had turbulence statistics (Table 1) similar to those expected in grid- or jet-stirred tanks, where turbulence is nearly homogeneous and isotropic (e.g. Hopfinger and Toly, 1976; Shy et al., 1997; Webster et al., 2004; Variano and Cowen, 2008). Mean velocities and Reynolds stresses $\overline{u'w'}$, where primes indicate fluctuating components of velocity, were small. The isotropy ratio was $w'_{rms}/u'_{rms} \approx 1$, where subscripts indicate root mean square, indicating that horizontal and vertical velocity fluctuations had similar magnitudes. Dissipation rates were reproducible and correlated with stirring frequency, and the highest dissipation rates at 350 rpm were representative of estuaries and flow over oyster reefs (Styles, 2015; Fuchs and Gerbi, 2016). The Kolmogorov length scale η_k ranged from approximately three times the larval length at 60 rpm to just smaller than the larvae at 350 rpm. Although the turbulence statistics were acceptable, the vorticity s.d. was ~20% lower than would be expected in isotropic turbulence at the observed dissipation rates (Taylor, 1935; Fuchs and Gerbi, 2016). Vorticity is the likely cue for behavioral responses to turbulence (Fuchs et al., 2015a), so reduced vorticity may have induced weaker or less frequent reactions to turbulence than previously observed.

Experiments

PIV data from still-water treatments demonstrated that larvae produced non-negligible turbulence by their swimming motions. At concentrations of ~7 to 11 larvae ml^{-1} (Table 2), mean dissipation rates averaged $\varepsilon=2.4\pm0.3\times10^{-8}$ m^2 s^{-3} even with no stirring. This value is low relative to dissipation rates observed over the continental shelf (Fuchs and Gerbi, 2016) but still cannot be considered as truly still water. We use this average larva-generated dissipation rate in reporting results for still-water treatments.

Behavior and turbulence changed little over the course of 3.5 h experiments, as demonstrated by linear regressions on data collected by PIV at 30-min intervals (Tables S3, S4). There were no temporal trends in the mean larval vertical velocity or percentage of larvae diving. Out of nine replicates, there were significant trends in the number of larvae observed in one still and one turbulent replicate and in the mean propulsive force in one still replicate. There were also significant trends in dissipation rate in one still and three turbulent replicates and in vorticity in two turbulent replicates. However, for all metrics, the effect magnitudes changed by ≤0.1% overall, indicating that changes in both behavior and turbulence were negligible. These results confirmed that larvae did not adapt to turbulence or food during the experiments. Larvae were also very similar in size and density across replicates (Table 2), so all PIV data were pooled for analysis of larval behavior.

Respiration

Overall, respiration and feeding rates were significantly affected by turbulence intensity, food availability and their interactions (Table 3A). Respiration rates were strongly affected by food and

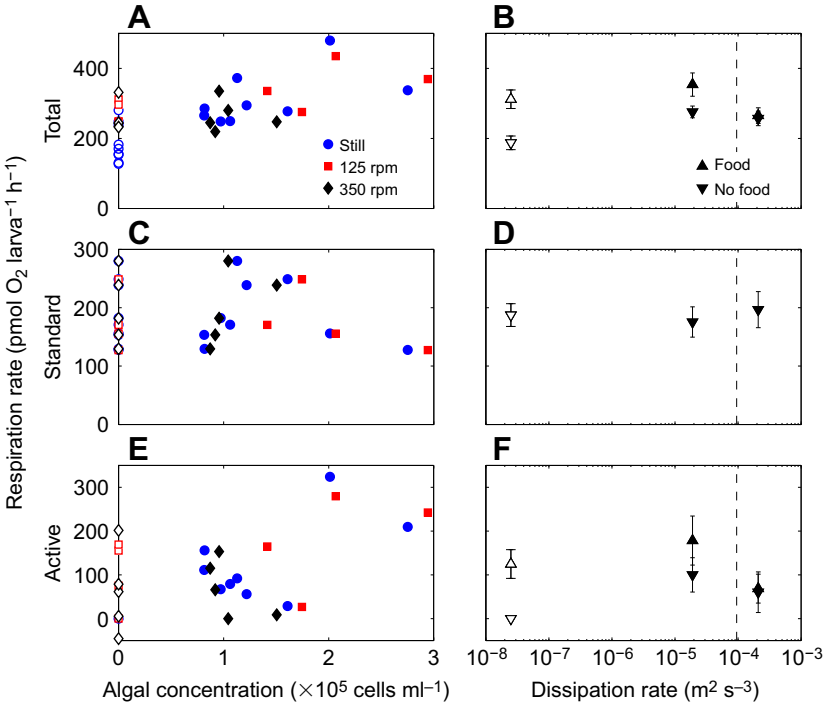

Fig. 1. Larval respiration rates were higher in the presence of food and/or turbulence. Total (*R*; A,B), standard (R_{std}; C,D) and active respiration rates (R_{active}; E,F). (A,C,E) All measurements versus initial algal concentration C_a; symbols indicate food (closed) or no-food (open) treatments in still water (blue circles), moderate turbulence (125 rpm; red squares) or strong turbulence (350 rpm; black diamonds). (B,D,F) Means±1 s.e.m. over replicates versus dissipation rate ε; symbols indicate food (upward triangle) and no-food (downward triangle) treatments in still water (open) and in turbulence (filled). Dissipation rates are shown as mean $\log_{10}\varepsilon$ in larval observations (still water) or in flow characterizations (turbulence). Vertical dashed lines indicate dissipation rate where larvae and Kolmogorov-scale eddies have the same length scale.

Journal of Experimental Biology

Journal of Experimental Biology (2017) 220, 3419-3431 doi:10.1242/jeb.161125

weakly affected by turbulence (Table 3B, Fig. 1). The mean total respiration rates were 67%, 28% and 3% higher with food than without food in still-water, 125 rpm and 350 rpm treatments, respectively (Fig. 1B), suggesting that feeding activity carries a high cost but is reduced or stops in strong turbulence. Even without food, however, respiration rates averaged 42% higher in turbulence than in still water. Standard respiration rates had a mean of 187± 18 pmol O_2 larva^{-1} h^{-1} and were uncorrelated with algal concentration or dissipation rate (Fig. 1C,D), indicating that variation in the total metabolic rate was driven by the cost of ciliary activity. When averaged by turbulence level, active respiration used 23% to 50% of the total metabolic cost (Fig. 1F), giving factorial aerobic scopes of 1.3 to 2.0; these values were highest with food in moderate turbulence where the mean algal concentration was highest.

Feeding

Food concentration and turbulence intensity also had interacting effects on feeding (Table 3B, Fig. 2). Ingestion rates increased linearly with food concentration, consistent with previous observations (Epifanio and Ewart, 1977), but the regression slope decreased with increasing turbulence intensity (Fig. 2A). Mean ingestion rates were highest at moderate turbulence intensity and lowest at high turbulence intensity (Fig. 2B), partly reflecting variation in food concentration. In still water, mean clearance rates were equivalent to specific clearance rates of ~3×10^4 body volumes day^{-1}, near the lowest value observed for plankton (Kiørboe and Jiang, 2012). Clearance rates were not significantly correlated with algal concentration at a given turbulence level (Fig. 2C), but clearance rate decreased steadily with dissipation rate (Fig. 2D), dropping by 67% from still water to the 350 rpm treatment.

Energetics

The selected, fitted models predicted that both respiration and ingestion rates increase with algal concentration but are highest at intermediate dissipation rates (Fig. 3). The selected models for respiration and ingestion were:

$$R^* = -92.6 - 4.50\times10^{-4}x - 146y - 1.62\times10^{-4}xy - 14.3x^2 \quad (16)$$

and

$$I^* = -3.85\times10^{-13} - 4.12\times10^{-2}x - 1.66\times10^{-13}y - 2.39\times10^{-2}xy - 1.06\times10^{-7}x^2 - 1.66\times10^{-14}y^2 - 1.28\times10^{-8}x^2y - 2.08\times10^{-3}xy^2, \quad (17)$$

where x is algal concentration and y is $\log_{10}$-scale dissipation rate ($\log_{10}\varepsilon$). The fitted models captured more of the observed variation in ingestion rate than in respiration rate (Fig. 3A,C), probably because ingestion was more significantly affected by both food availability and turbulence (Table 3). The fitted models indicated that both R^* and I^* – and, by extension, clearance rate – had dome-shaped relationships with dissipation rate. This prediction for clearance rate differs from the observed F, which decreased with ε (Fig. 2D), and may be an artifact of lacking data in weak turbulence.

Estimates of the net rate of energy gain (Eqn 1) indicated that larvae had a net energy loss in most flasks (Fig. 4A), achieving an energy gain in only a handful of replicates with food in still water or moderate turbulence. Like respiration and ingestion rates, the fitted E^* increased with algal concentration and was highest at intermediate dissipation rates (Fig. 4B). The model predicts that larvae could achieve a net energy gain only when $C_a \geq 1.1\times10^5$ cells ml^{-1} and $\varepsilon \leq 4.6\times10^{-5}$ m^2 s^{-3}. This upper limit on dissipation rate is associated with a Kolmogorov scale of $\eta_k \approx 380$ µm, slightly larger than the mean larval length of d=320 µm, and may indicate the size of fluid motions that prevent formation of feeding currents.

Swimming behavior and efficiency

PIV data showed that larvae sank or dove more frequently and swam with more propulsive force as dissipation rates increased (Fig. 5). All larvae used more propulsive force $|\mathbf{F}_v|$ in response to vorticity-induced body rotation (Fig. 5C–F), but there was more scatter for sinking or diving larvae, of which there were fewer. Propulsive force is generally aligned with the larval body axis, and flow-induced rotation reduces the vertical component of propulsive force that swimming larvae use to offset gravitational sinking. By expending more effort, swimming larvae were able to maintain vertical velocities w_b near zero and avoid gyrotactic sinking (Fig. 5G).

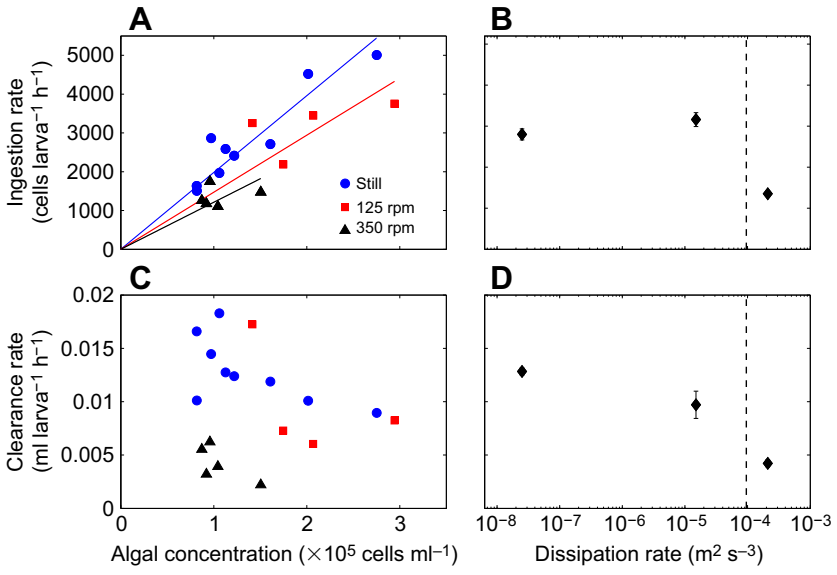

Fig. 2. Larval feeding was inhibited by strong turbulence. Larval ingestion rates I (A,B) and clearance rates F (C,D). (A,C) All measurements versus initial algal concentration C_a; symbols indicate still water (blue circles), moderate turbulence (125 rpm; red squares) or strong turbulence (350 rpm; black triangles). Solid lines (A) are linear regressions forced through the origin (still, R^2=0.87, $P<10^{-7}$; 125 rpm, R^2=0.52, P=0.0071; 350 rpm, R^2=0.33, P=0.0029). No regressions were significant for clearance rate. (B,D) Means±1 s.e. over replicates versus dissipation rate ε. Dissipation rates and vertical lines as in Fig. 1B,D.

Journal of Experimental Biology (2017) 220, 3419-3431 doi:10.1242/jeb.161125

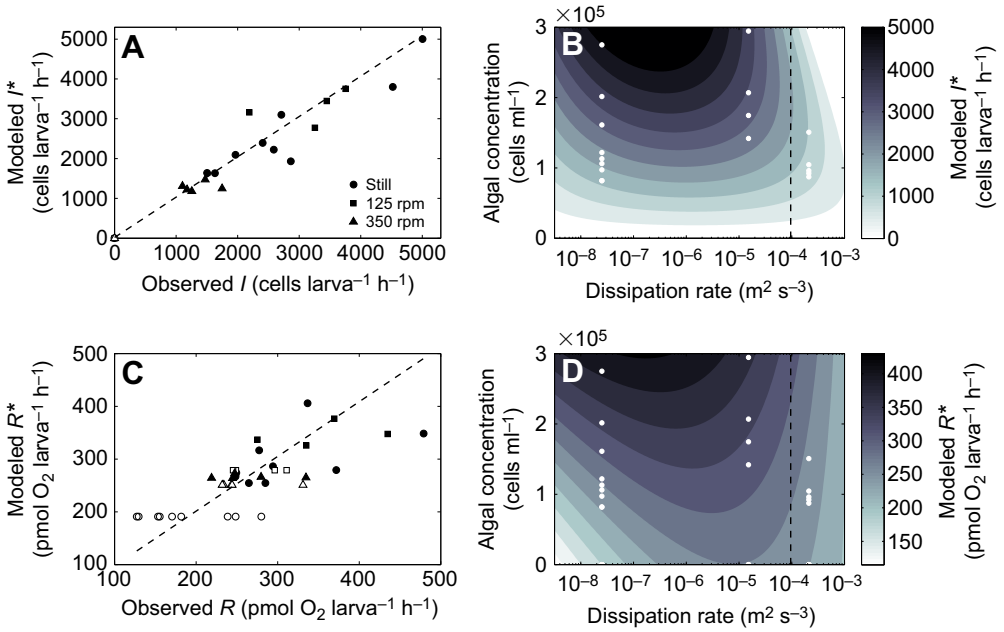

Fig. 3. Predicted ingestion and respiration rates peak at low dissipation rates. Model fits for oyster larval ingestion rates (I^*; A,B) and respiration rates (R^*; C,D). (A,C) Model-predicted versus observed rates with regression lines (dashed; A, R^2=0.96, $P<10^{-24}$; C, R^2=0.57, $P<10^{-7}$). Symbols indicate still water (circles), moderate turbulence (125 rpm; squares) or strong turbulence (350 rpm; triangles) and food presence (closed) or absence (open). (B,D) Model-predicted rates versus algal concentration C_a and dissipation rate ε. Vertical dashed lines as in Fig. 1B,D. White dots indicate locations of data points used for fitting.

However, the added swimming effort and flow-induced rotation increased the horizontal component of propulsive force, and the larval vector velocity $\mathbf{V}_b$ of swimming larvae increased with dissipation rate (Fig. 5G). As a result, the Reynolds numbers increased from Re_p≈0.3 in still water to 1.5 in strong turbulence (Fig. S1A). In contrast, the velocities of sinking/diving larvae were always dominated by vertical motion, and Reynolds numbers remained fairly steady at Re_p≈3.0 (Fig. S1B).

Swimming efficiency appeared to vary with both swimming behavior and feeding activity (Fig. 6, Fig. S1). Mirroring the changes in $\mathbf{F}_v$ and $\mathbf{V}_b$ (Fig. 5E–H), power output P_o increased with and was highly correlated with dissipation rate, particularly for swimming larvae (Fig. 6A, Fig. S1C). In contrast, the active metabolic rate E_{active} had a dome-shaped relationship with dissipation rate (Fig. 6B) and was highest in moderate turbulence (Fig. 1E,F). Some of these activity costs probably were incurred by ciliary feeding rather than swimming, given that ingestion rates were highest in moderate turbulence (Fig. 2B). Swimming efficiency η_s was concave up versus dissipation rate, ranging from ∼0.0013 in moderate turbulence to ∼0.05 in strong turbulence for both behaviors (Fig. 6C, Fig. S1E,F). The different functional responses of power output and swimming efficiency suggest that ciliary feeding carries added metabolic costs that cannot be predicted by swimming metrics.

Although swimming efficiency followed a similar pattern for both behaviors, the cost of transport was more variable. For swimming larvae, the cost of transport was lowest in strong turbulence, where larvae gained in efficiency, whereas for sinking/diving larvae, the cost of transport was lowest in still water, where descents were most passive (Fig. S1G,H). The mean cost of transport was 1040 J m^{-1} kg^{-1} for swimming larvae and 180 J m^{-1} kg^{-1} for sinking or diving larvae, indicating that the cost of swimming upward against the pull of gravity was approximately six times higher than the cost of descending.

Particle capture efficiency

Turbulence strongly affected all aspects of particle capture (Fig. 7). In flasks observed by PIV, clearance rates were negatively correlated with dissipation rate and dropped by 75% from still water to the 350 rpm treatment (Fig. 7A). Encounter rates were positively correlated with dissipation rate and increased by an order of magnitude above the $\varepsilon|_{\eta_k=d}$ threshold (Fig. 7B). This increase reflects nearly equal contributions from encounter rates that are due to turbulence β_t and those that are due to behavior β_b. Above the $\varepsilon|_{\eta_k=d}$ threshold, β_t increased sharply because of its changing dependence on dissipation rate (Eqn 8), whereas β_b increased sharply because high vorticity induced stronger swimming and body rotation, increasing the larval vector velocity $\mathbf{V}_b$ (Eqn 9). The estimated capture efficiency dropped by 84% from still water to the highest turbulence intensity, with a more negative slope at higher dissipation rates (Fig. 7C). The decline in clearance rate with ε suggests that the positive effects of turbulence on encounter rate

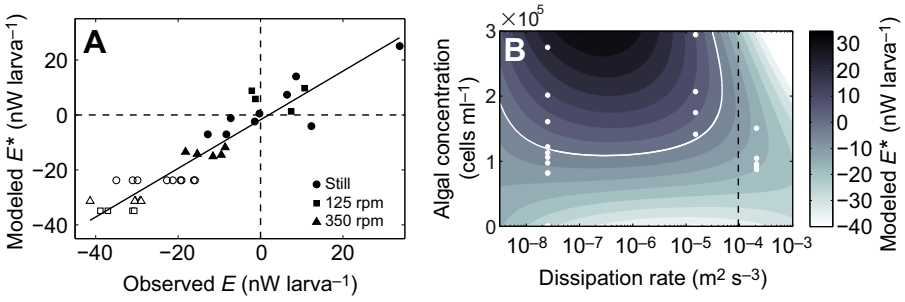

Fig. 4. Larvae lose energy in strong turbulence. Net rate of energy gain E for oyster larvae. (A) Model-predicted versus observed values with regression line (R^2=0.88, $P<10^{-16}$). Symbols as in Fig. 3. (B) Model-predicted values versus algal concentration C_a and dissipation rate ε. Vertical dashed lines as in Fig. 1B,D; white dots as in Fig. 3B,D. White line indicates conditions with no net energy gain. Lighter shading (below and to right of white line) indicates net energy loss.

Journal of Experimental Biology (2017) 220, 3419-3431 doi:10.1242/jeb.161125

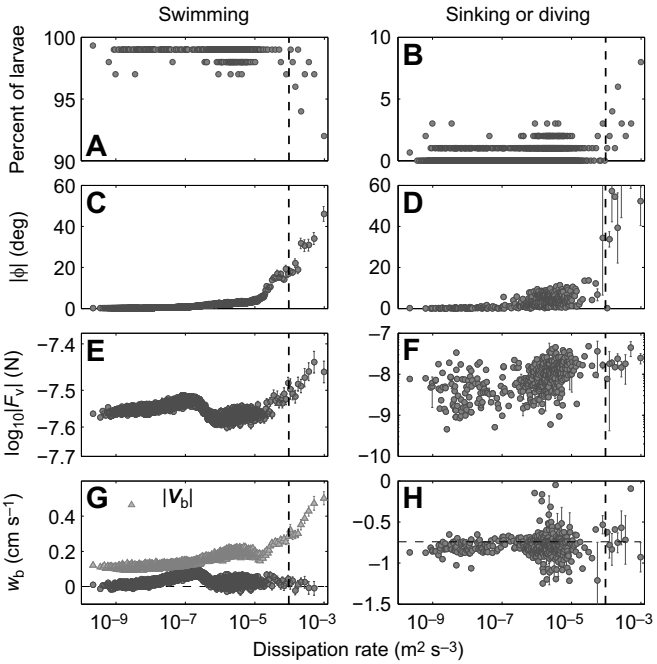

Fig. 5. Turbulence induces larval rotation, stronger swimming and diving. Oyster larval swimming behavior versus dissipation rate ε. Instantaneous measurements on individual larvae are binned by dissipation rate (N=100) and shown as means±1 s.e.m. Separate estimates are shown for larvae propelling themselves upward (left) and downward (right) relative to body axis. (A,B) Percent of larvae in each behavior mode. (C,D) Angle $|\phi|$ of larval rotation due to vorticity. (E,F) Magnitude of propulsive force $|\mathbf{F}_v|$. (G,H) Larval vertical velocity w_b and vector velocity magnitude $|\mathbf{V}_b|$ (G only) due to behavior. Horizontal dashed lines indicate neutral buoyancy (G) and mean terminal sinking velocity w_T (H). Vertical dashed lines as in Fig. 1B,D. All trends are significant except w_b versus ε for sinking/diving larvae; regression lines omitted for clarity. Additional behavior results given in Fig. S1.

were always outweighed by its negative effects on capture efficiency, particularly when Kolmogorov-scale eddies were near the larval size.

DISCUSSION

This study demonstrates that energy gain by larval oysters is fundamentally altered by turbulence, which induces metabolically costly behaviors while inhibiting food capture. Our results suggest that pediveligers would be unable to maintain their body mass at dissipation rates representative of coastal waters, even when food concentrations are very high. Body maintenance costs are a bare minimum for survival; to succeed, larvae must also gain enough energy to develop through metamorphosis (Hoegh-Guldberg and Emlet, 1997; Marsh et al., 1999), reach a suitable habitat (Bennett and Marshall, 2005; Wilkin and Jeffs, 2011) and survive after settlement (Phillips, 2002; Pechenik, 2006). A net loss of energy in strong turbulence could contribute to high larval mortality rates. *Crassostrea virginica* live up to 20 years and produce ~10^6 eggs per spawn (Buroker, 1983; Gallager and Mann, 1986), so that the probability of a fertilized egg surviving to reproduction is $\leq 10^{-7}$. Extreme larval mortality has been attributed to starvation, predation and errant transport (Thorson, 1950), but starvation may be more common than expected because larvae are unable to gain energy in turbulence.

We previously predicted that larval metabolic rates would increase in turbulence because flow induces swimming behaviors with high power outputs (Fuchs et al., 2015b), but this study showed that metabolic costs vary with both swimming and feeding. The activity costs of feeding in still water were as high as those of swimming with more effort in turbulence, but feeding activity was reduced or stopped in turbulence where clearance rates were low (Figs 1D and 2D). It is impossible to determine whether larvae stopped feeding because capture efficiency dropped, or vice versa. However, feeding may have been reduced in turbulence simply because all ciliary activity was diverted to stronger swimming, enabling larvae to avoid vorticity-induced gyrotactic sinking. These data suggest that although larvae swim and feed at the same time, they cannot do both at full capacity simultaneously, and vertical positioning takes precedence in turbulence.

We also expected swimming efficiency to decrease with dissipation rate as flow-induced behaviors caused an increase in the particle Reynolds number, but in fact swimming efficiency had a concave-up relationship with dissipation rate and was highest in strong turbulence (Fig. 6). Swimming efficiency is computed from active metabolic rate without separating the costs of swimming and food capture, and its convexity may indicate that these two ciliary activities had opposite relationships with turbulence. Ciliary feeding could become less metabolically efficient in turbulence if a drop in capture efficiency forced larvae to expend more energy handling food. Although less intuitive, swimming could become more efficient in turbulence as larvae are rotated by fluid motions. In still water, larvae hover with just enough propulsive force to offset gravitational sinking. In turbulence, vorticity rotates the larvae and directs the propulsive force more horizontally, so more effort is required to maintain the vertical thrust component to avoid sinking. The horizontal component of propulsive force is opposed only by drag and other forces that are small relative to the gravitational force (Fuchs et al., 2015b), and larvae gain speed via horizontal motion (Fig. 5) (e.g. Grünbaum and Strathmann, 2003; Chan, 2012). Both the increased propulsive force and speed raise the power output, but horizontal swimming is less metabolically costly than swimming vertically against gravity, and rotation enables larvae to swim more efficiently.

Ciliary swimmers are unique in using the same appendages to swim and feed simultaneously, yet oyster larvae generally conformed to allometric energetic relationships for ectotherms. Swimming efficiencies were within the range predicted by simple scaling arguments for ciliated organisms (Sleigh and Blake, 1977). The estimated cost of transport was lower than observed in smaller *Paramecium* (Katsu-Kimura et al., 2009) and higher than observed in larger copepods *Pleuromamma xiphias* (Morris et al., 1985), fitting the general pattern of decreasing cost of transport with size (Tucker, 1975; Morris et al., 1985). In fact, the mean cost of transport for swimming larvae (mCOT=2.1×10^{-5} J m^{-1} larva^{-1}) was very close to the empirical allometric prediction for fish larvae if they had the same mass as oyster larvae (mCOT=3.1×10^{-5} J m^{-1}; Bale et al., 2014). Although efficiency and cost may have been predictable based on size, the factorial aerobic scope was not; oyster larvae had a maximum FAS of 2.0, comparable to that of fish larvae and shallow-water squid with up to 10^6 times more mass (Bartol et al., 2001; Killen et al., 2007). This measure of performance indicates that despite their small size and weak propulsion mechanism, larvae can greatly increase their ciliary activity to double the total metabolic rate.

Metabolic costs must be offset by energy gained from feeding, which is sensitive to the energy content of algal cells and can include other nutrition sources. Late-stage *C. virginica* larvae consume phytoplankton with d=0.5 to 30 µm in proportion to their concentrations in natural assemblages (Baldwin and Newell, 1995).

Journal of Experimental Biology (2017) 220, 3419-3431 doi:10.1242/jeb.161125

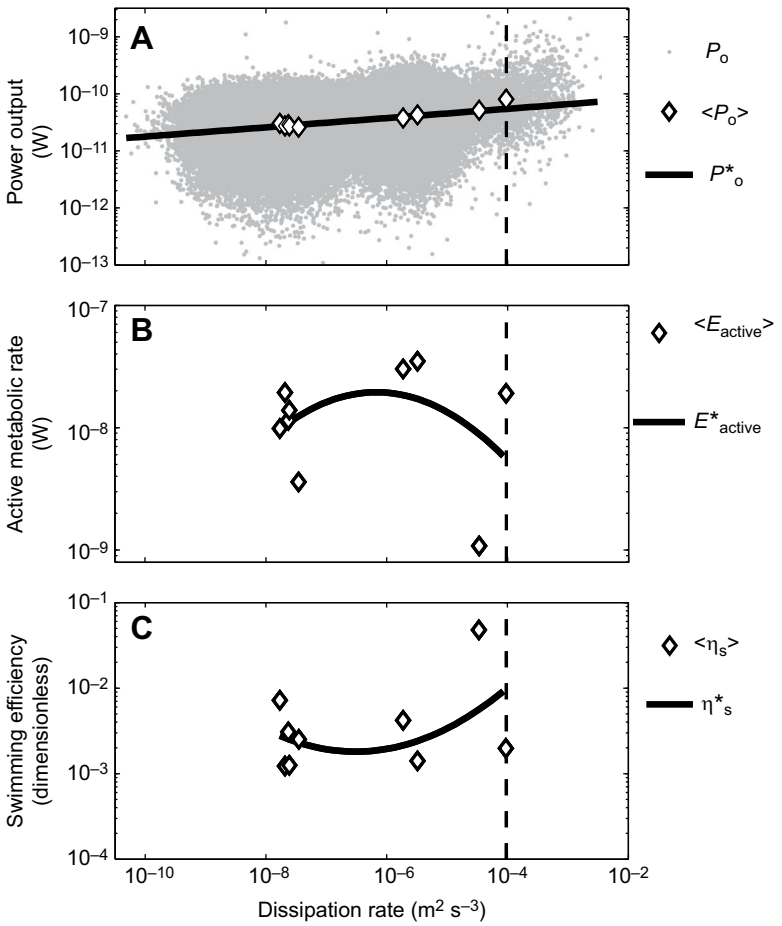

Fig. 6. Larval swimming efficiency is concave up versus dissipation rate. Oyster larval power output P_o, active metabolic rate E_{active} and swimming efficiency η_s versus dissipation rate ε in flasks observed with PIV. Symbols are instantaneous measurements on individual larvae (gray dots), means of instantaneous measurements versus mean $\log_{10}\varepsilon$ for each replicate (diamonds; indicated by angle brackets), and fitted estimates (black lines; indicated by asterisks). (A) Power output; line is linear regression of instantaneous P_o versus $\log_{10}\varepsilon$ (R^2=0.08, $P<10^{-16}$). (B) Active metabolic rate; line is quadratic fit of E_{active} versus $\log_{10}\varepsilon$. (C) Swimming efficiency (Eqn 3); symbols are computed from replicate means, and solid line is computed from fitted estimates. Vertical dashed lines as in Fig. 1B,D.

Larger cells contain more energy; for example, *Tetraselmis* sp., a 12-µm flagellate, has 27 times the energy content of 5-µm *I. galbana* used here (Reed Mariculture). However, larger cells are less abundant, and larvae feed on them at lower rates, so total nutritional gains may be unaffected by cell size distribution (Epifanio and Ewart, 1977). Oyster larvae also consume bacteria and small heterotrophs, but clearance rates on these groups are lower than on phytoplankton (Baldwin and Newell, 1991). It is more difficult to account for metabolic energy gained through uptake of dissolved organic matter such as amino acids (Manahan, 1983, 1990). Although some lecithotrophic larvae can gain biomass on dissolved organic matter alone (Jaeckle and Manahan, 1992; Shilling and Manahan, 1994), there is no evidence that *C. virginica* larvae can survive or grow to competency without particulate food. Still, we may have underestimated E_{food} by only accounting for consumed phytoplankton.

Any underestimate in the metabolic gains from food could have been offset by our conservative use of a constant assimilation efficiency (η_a=0.54). Assimilation efficiency is species specific but decreases with food concentration in other veligers (*Ostrea edulis* and *Mytilus edulis*; Jespersen and Olsen, 1982; Crisp et al., 1985). Here we used an assimilation efficiency measured previously for *C. virginica* larvae fed *I. galbana* at a concentration of 5×10^4 cells ml^{-1} (Reinfelder and Fisher, 1994). In the present experiment, concentrations were 8.2×10^4 to 2.9×10^5 cells ml^{-1}, approximately two to six times higher than those used by Reinfelder and Fisher (1994). A comparable increase in algal concentrations, i.e. from 5×10^4 to 3×10^5 cells ml^{-1}, reduced the assimilation efficiencies of *M. edulis* and *O. edulis* by ~9% and ~44%, respectively (Crisp et al., 1985). If η_a varies similarly with algal concentration in *C. virginica*, assimilation efficiencies may have been overestimated here by 9 to 44% and could have been as low as η_a=0.49 to 0.30 in our experiments. Overall, the predicted range of conditions where larvae could gain energy may be overly optimistic.

Our results suggest that oyster larvae are unable to gain energy in strong turbulence partly because turbulence inhibits food capture more than it enhances food encounter rates. However, our use of only two turbulence treatments leaves some uncertainty in whether feeding could be enhanced by weaker turbulence ($\varepsilon\approx10^{-7}$ to 10^{-6} m^2 s^{-3}), where the positive effects of turbulence on encounter rates may outweigh the negative effects on capture efficiency (MacKenzie et al., 1994). Copepod studies suggest that weak turbulence can have a net positive effect on ambush feeding but not on suspension feeding (Saiz and Kiørboe, 1995; Saiz et al., 2003), and our results for suspension-feeding oyster larvae are equivocal. The measured clearance rate decreased with $\log_{10}\varepsilon$, whereas the fitted model gave a dome-shaped relationship between ingestion rate and dissipation rate, implying that clearance rates should peak at $\varepsilon\approx10^{-6}$ m^2 s^{-3}. This discrepancy arises from a lack of data in weak turbulence, and we cannot rule out enhancement of feeding at low dissipation rates.

Here we omitted weak turbulence treatments in favor of resolving how energetics vary around the $\varepsilon|_{\eta_k=d}$ threshold, where larvae and Kolmogorov-scale eddies are of similar size. Intriguingly, near this threshold the decrease in food capture efficiency with dissipation rate appeared to accelerate (Fig. 7). This result suggests that capture efficiency is reduced in turbulence not just by higher relative speed of food particles, but also by greater degradation of feeding currents

Journal of Experimental Biology (2017) 220, 3419-3431 doi:10.1242/jeb.161125

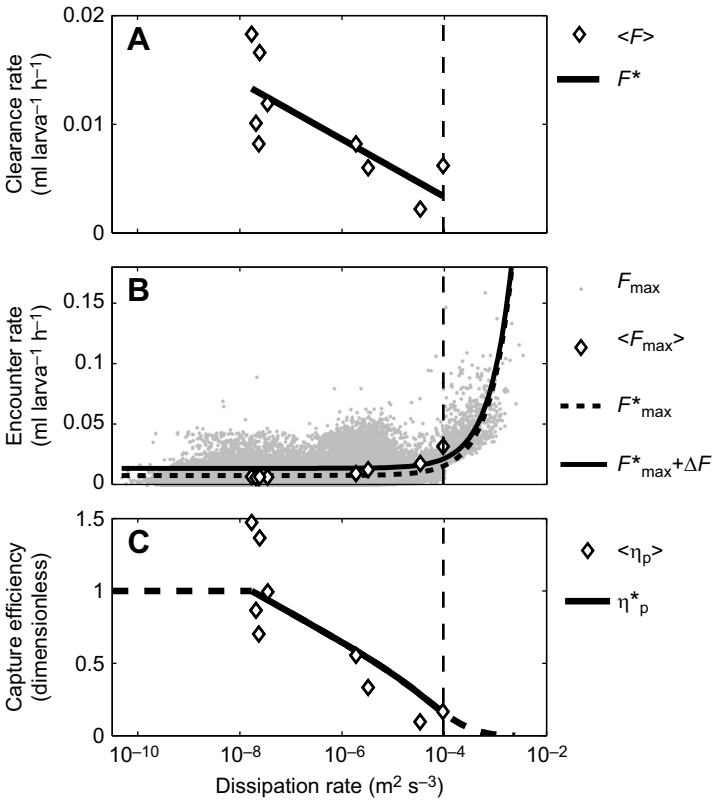

Fig. 7. Turbulence enhances food encounter rates but reduces capture efficiency. Oyster larval clearance rate F, encounter rate F_{max} and particle capture efficiency η_p versus dissipation rate ε in flasks observed with PIV. Symbols as in Fig. 6. (A) Clearance rates; line is linear regression of F versus $\log_{10}\varepsilon$ (R^2=0.60, P=0.014). (B) Encounter rates; lines are linear regression of instantaneous F_{max} versus ε (dotted line; R^2=0.14, $P<10^{-16}$) and correction $F^*_{max}+\Delta F$, where ΔF=0.01 (solid line; see Materials and methods for details). (C) Particle capture efficiency (Eqn 15); symbols are computed from replicate means, and line is computed from fitted estimates. Vertical dashed lines as in Fig. 1B,D.

as the smallest eddies approach the larval size. We cannot disentangle these effects in our data, because the PIV resolution precluded visualizing the feeding currents. Recently developed micro-PIV techniques (Gemmell et al., 2014; Kiørboe et al., 2014) may soon enable larval observations at the scale needed to quantify how feeding currents are altered by turbulence.

The turbulence intensities used here are common in coastal regions, and our results indicate that larval energetics are strongly impacted by physics. At sea, turbulence intensity varies with tidal currents, winds and stratification, but dissipation rates are highest in the wind-affected surface layer, bottom boundary layer and in shallow water near coastlines. In inlets, in estuaries and over the continental shelf, dissipation rates are frequently $\varepsilon\approx10^{-5}$ to 10^{-4} m^2 s^{-3} and can reach 10^{-3} m^2 s^{-3} (Fuchs and Gerbi, 2016). Oyster habitats are particularly turbulent because of the rough bottom topography of oyster reefs, which generates dissipation rates of $\varepsilon\approx10^{-3}$ m^2 s^{-3} during flood and ebb tides (Styles, 2015). Our fitted model indicated that competent oyster larvae could gain energy only when $\varepsilon\leq5\times10^{-5}$ m^{-2} s^{-3}. Comparing this value with observed dissipation rates, larvae in coastal waters may suffer a net energy loss throughout much of the tidal cycle.

There are two mechanisms by which smaller, pre-competent larvae could gain energy in turbulence where larger, competent larvae cannot. Competent larvae responded to turbulence by swimming with more effort, incurring high activity costs, while their food capture was impeded by increased speed relative to particles and/or erosion of feeding currents by eddy motions. Pre-competent larvae may have lower activity costs in turbulence because they lack statocysts – the probable mechanism for sensing fluid motion (Fuchs et al., 2015a) – until the pediveliger stage (Ellis and Kempf, 2011) and should be unreactive to turbulence, incurring no extra swimming costs. Pre-competent larvae are also smaller relative to the Kolmogorov scale and may have a size refuge from erosion of feeding currents. At half the larval size used here, the $\varepsilon|_{\eta_k=d}$ threshold is 16 times higher ($\varepsilon|_{\eta_k=d}=1.5\times10^{-3}$ m^2 s^{-3}), so larvae and their feeding currents would be smaller than eddy motions under a wider range of coastal conditions. Overall, we predict that rates of turbulence-induced starvation mortality increase with larval size; statocysts develop with age and enable flow-induced behaviors with high metabolic costs, while larval growth relative to the Kolmogorov scale may make it more difficult to maintain feeding currents.

Acknowledgements

D. Merritt and S. Alexander at Horn Point Laboratory kindly provided the oyster larvae. E. J. Hunter assisted with PIV image processing. Coulter Counter access was provided by the Rutgers Environmental Biophysics and Molecular Ecology Laboratory. J. Grassle provided helpful comments on the manuscript.

Competing interests

The authors declare no competing or financial interests.

Author contributions

Conceptualization: H.L.F., D.K.A.; Methodology: H.L.F., A.J.C.; Software: H.L.F.; Validation: H.L.F.; Formal analysis: H.L.F.; Investigation: H.L.F., J.A.S., A.J.C.; Resources: H.L.F., D.K.A.; Data curation: H.L.F.; Writing - original draft: H.L.F.; Writing - review & editing: H.L.F.; Visualization: H.L.F.; Supervision: H.L.F.; Project administration: H.L.F.; Funding acquisition: H.L.F.

Funding

This work was funded in part by a Rutgers Research Council grant to H.L.F. J.A.S. was supported by a Graduate Assistantship from the Institute of Marine and Coastal Sciences, Rutgers, The State University of New Jersey.

Data availability

Data are available from the Dryad Digital Repository (Fuchs et al., 2017): http://dx.doi.org/10.5061/dryad.7rr7m

Supplementary information

Supplementary information available online at http://jeb.biologists.org/lookup/doi/10.1242/jeb.161125.supplemental

References

Adrian, R. J. (1991). Particle-imaging techniques for experimental fluid mechanics. *Annu. Rev. Fluid Mech.* **23**, 261-304.

Alcaraz, M. (1997). Copepods under turbulence: grazing, behavior and metabolic rates. *Sci. Mar.* **61** Suppl. 1, 177-195.

Baker, P. (1994). Competency to settle in oyster larvae, *Crassostrea virginica*: wild versus hatchery-reared larvae. *Aquaculture* **122**, 161-169.

Baldwin, B. S. and Newell, R. I. E. (1991). Omnivorous feeding by planktotrophic larvae of the eastern oyster *Crassostrea virginica*. *Mar. Ecol. Prog. Ser.* **78**, 285-301.

Baldwin, B. S. and Newell, R. I. E. (1995). Feeding rate responses of oyster larvae (*Crassostrea virginica*) to seston quality and composition. *J. Exp. Mar. Biol. Ecol.* **189**, 77-91.

Bale, R., Hao, M., Bhalla, A. P. S. and Patankar, N. A. (2014). Energy efficiency and allometry of movement of swimming and flying animals. *Proc. Natl. Acad. Sci.* **111**, 7517-7521.

Bartol, I. K., Mann, R. and Patterson, M. R. (2001). Aerobic respiratory costs of swimming in the negatively buoyant brief squid *Lolliguncula brevis*. *J. Exp. Biol.* **204**, 3639-3653.

Bennett, C. E. and Marshall, D. J. (2005). The relative energetic costs of the larval period, larval swimming and metamorphosis for the ascidian *Diplosoma listerianum*. *Mar. Freshwater Behav. Physiol.* **38**, 21-29.

Burnham, K. P. and Anderson, D. R. (2002). *Model Selection and Multimodel Inference*, 2nd edn. New York: Springer.

Buroker, N. E. (1983). Population genetics of the American oyster *Crassostrea virginica* along the Atlantic coast and the Gulf of Mexico. *Mar. Biol.* **75**, 99-112.

Catton, K. B., Webster, D. R., Brown, J. and Yen, J. (2007). Quantitative analysis of tethered and free-swimming copepodid flow fields. *J. Exp. Biol.* **210**, 299-310.

Chan, K. Y. K. (2012). Biomechanics of larval morphology affect swimming: insights from the sand dollars *Dendraster excentricus*. *Integr. Comp. Biol.* **52**, 458-469.

Clarke, A. and Fraser, K. P. P. (2004). Why does metabolism scale with temperature? *Funct. Ecol.* **18**, 243-251.

Clay, T. W. and Grünbaum, D. (2010). Morphology-flow interactions lead to stage-selective vertical transport of larval sand dollars in shear flow. *J. Exp. Biol.* **213**, 1281-1292.

Crawford, D. W. (1992). Metabolic cost of motility in planktonic protists: theoretical considerations on size scaling and swimming speed. *Microb. Ecol.* **24**, 1-10.

Crisp, D. J., Yule, A. B. and White, K. N. (1985). Feeding by oyster larvae: the functional response, energy budget and a comparison with mussel larvae. *J. Mar. Biol. Assoc. UK* **65**, 759-783.

Doron, P., Bertuccioli, L., Katz, J. and Osborn, T. R. (2001). Turbulence characteristics and dissipation estimates in the coastal ocean bottom boundary layer from PIV data. *J. Phys. Oceanogr.* **31**, 2108-2134.

Durham, W. M., Kessler, J. O. and Stocker, R. (2009). Disruption of vertical motility by shear triggers formation of thin phytoplankton layers. *Science* **323**, 1067-1070.

Ellis, I. and Kempf, S. C. (2011). Characterization of the central nervous system and various peripheral innervations during larval development of the oyster *Crassostrea virginica*. *Invertebr. Biol.* **130**, 236-250.

Emlet, R. B., Strathman, R. R. and Strickler, J. R. (1985). Gravity, drag, and feeding currents of small zooplankton. *Science* **228**, 1016-1017.

Epifanio, C. E. and Ewart, J. (1977). Maximum ration of four algal diets for the oyster *Crassostrea virginica* Gmelin. *Aquaculture* **11**, 13-29.

Fenchel, T. and Ockelmann, K. W. (2002). Larva on a string. *Ophelia* **56**, 171-178.

Fuchs, H. L. and Gerbi, G. P. (2016). Seascape-level variation in turbulence- and wave-generated hydrodynamic signals experienced by plankton. *Progr. Oceanogr.* **141**, 109-129.

Fuchs, H. L. and Reidenbach, M. A. (2013). Biophysical constraints on optimal patch lengths for settlement of a reef-building bivalve. *PLoS ONE* **8**, e71506.

Fuchs, H. L., Mullineaux, L. S. and Solow, A. R. (2004). Sinking behavior of gastropod larvae (*Ilyanassa obsoleta*) in turbulence. *Limnol. Oceanogr.* **49**, 1937-1948.

Fuchs, H. L., Neubert, M. G. and Mullineaux, L. S. (2007). Effects of turbulence-mediated larval behavior on larval supply and settlement in tidal currents. *Limnol. Oceanogr.* **52**, 1156-1165.

Fuchs, H. L., Hunter, E. J., Schmitt, E. L. and Guazzo, R. A. (2013). Active downward propulsion by oyster larvae in turbulence. *J. Exp. Biol.* **216**, 1458-1469.

Fuchs, H. L., Christman, A. J., Gerbi, G. P., Hunter, E. J. and Diez, F. J. (2015a). Directional flow sensing by passively stable larvae. *J. Exp. Biol.* **218**, 2782-2792.

Fuchs, H. L., Gerbi, G. P., Hunter, E. J., Christman, A. J. and Diez, F. J. (2015b). Hydrodynamic sensing and behavior by oyster larvae in turbulence and waves. *J. Exp. Biol.* **218**, 1419-1432.

Fuchs, H. L., Specht, J. A., Adams, D. K. and Christman, A. J. (2017). Data from: Turbulence induces metabolically costly behaviors and inhibits food capture in oyster larvae, causing net energy loss. *Dryad Digital Repository*.

Galbraith, P. S., Browman, H. I., Racca, R. G., Skiftesvik, A. B. and Saint-Pierre, J.-F. (2004). Effect of turbulence on the energetics of foraging in Atlantic cod *Gadus morhua* larvae. *Mar. Ecol. Prog. Ser.* **281**, 241-257.

Gallager, S. M. (1988). Visual observations of particle manipulation during feeding in larvae of a bivalve mollusc. *Bull. Mar. Sci.* **43**, 344-365.

Gallager, S. M. (1993). Hydrodynamic disturbances produced by small zooplankton: case study for the veliger larva of a bivalve mollusc. *J. Plankton Res.* **15**, 1277-1296.

Gallager, S. M. and Mann, R. (1986). Growth and survival of larvae of *Mercenaria mercenaria* (L.) and *Crassostrea virginica* (Gmelin) relative to broodstock conditioning and lipid content of eggs. *Aquaculture* **56**, 105-121.

Gemmell, B. J., Jiang, H. and Buskey, E. J. (2014). A new approach to micro-scale particle image velocimetry (μPIV) for quantifying flows around free-swimming zooplankton. *J. Plankton Res.* **36**, 1396-1401.

Gerritson, J. (1984). Size efficiency reconsidered: a general foraging model for free-swimming aquatic animals. *Am. Nat.* **123**, 450-467.

Gnaiger, E. (1983). Calculation of energetic and biochemical equivalents of respiratory oxygen consumption. In *Polarographic Oxygen Sensors: Aquatic and Physiological Applications* (ed. E. Gnaiger and H. Forstner), pp. 337-345. New York: Springer-Verlag.

Grünbaum, D. and Strathmann, R. R. (2003). Form, performance and trade-offs in swimming and stability of armed larvae. *J. Mar. Res.* **61**, 659-691.

Guseva, K., Feudel, U. and Tél, T. (2013). Influence of the history force on inertial particle advection: Gravitational effects and horizontal diffusion. *Phys. Rev. E* **88**, 042909.

Hoegh-Guldberg, O. and Emlet, R. B. (1997). Energy use during the development of a lecithotropic and a planktotophic echinoid. *Biol. Bull.* **192**, 27-40.

Hoegh-Guldberg, O. and Manahan, D. T. (1995). Coulometric measurement of oxygen consumption during development of marine invertebrate embryos and larvae. *J. Exp. Biol.* **198**, 19-30.

Hopfinger, E. J. and Toly, J.-A. (1976). Spatially decaying turbulence and its relation to mixing across density interfaces. *J. Fluid Mech.* **78**, 155-175.

Hubbard, A. B. and Reidenbach, M. A. (2015). Effects of larval swimming behavior on the dispersal and settlement of the eastern oyster *Crassostrea virginica*. *Mar. Ecol. Prog. Ser.* **535**, 161-176.

Jaeckle, W. B. and Manahan, D. T. (1992). Experimental manipulations of the organic composition of seawater: implications for studies of energy budgets in marine invertebrate larvae. *J. Exp. Mar. Biol. Ecol.* **1992**, 273-284.

Jespersen, H. and Olsen, K. (1982). Bioenergetics in veliger larvae of *Mytilus edulis* L. *Ophelia* **21**, 101-113.

Jonsson, P. R., André, C. and Lindegarth, M. (1991). Swimming behaviour of marine bivalve larvae in a flume boundary-layer flow: evidence for near-bottom confinement. *Mar. Ecol. Prog. Ser.* **79**, 67-76.

Jumars, P. A., Trowbridge, J. H., Boss, E. and Karp-Boss, L. (2009). Turbulence-plankton interactions: a new cartoon. *Mar. Ecol.* **30**, 133-150.

Katsu-Kimura, Y., Nakaya, F., Baba, S. A. and Mogami, Y. (2009). Substantial energy expenditure for locomotion in ciliates verified by means of simultaneous measurement of oxygen consumption rate and swimming speed. *J. Exp. Biol.* **212**, 1819-1824.

Kessler, J. O. (1986). The external dynamics of swimming micro-organisms. *Prog. Phycol. Res.* **4**, 257-291.

Khalitov, D. A. and Longmire, E. K. (2002). Simultaneous two-phase PIV by two-parameter phase discrimination. *Exp. Fluids* **32**, 252-268.

Kiger, K. T. and Pan, C. (2000). PIV technique for the simultaneous measurement of dilute two-phase flows. *J. Fluids Eng.* **122**, 811-818.

Killen, S. S., Costa, I., Brown, J. A. and Gamperl, A. K. (2007). Little left in the tank: metabolic scaling in marine teleosts and its implications for aerobic scope. *Proc. R. Soc. B* **274**, 431-438.

Kiørboe, T. and Jiang, H. (2012). To eat and not be eaten: optimal foraging behaviour in suspension feeding copepods. *J. R. Soc. Interface* **10**, 20120693.

Kiørboe, T. and Saiz, E. (1995). Planktivorous feeding in calm and turbulent environments, with emphasis on copepods. *Mar. Ecol. Prog. Ser.* **122**, 135-145.

Kiørboe, T., Jiang, H., Gonçalves, R. J., Nielsen, L. T. and Wadhwa, N. (2014). Flow disturbances generated by feeding and swimming zooplankton. *Proc. Natl. Acad. Sci.* **111**, 11738-11743.

Koehl, M. A. R. and Cooper, T. (2015). Swimming in an unsteady world. *Integr. Comp. Biol.* **55**, 683-697.

Lazier, J. R. N. and Mann, K. H. (1989). Turbulence and the diffusive layers around small organisms. *Deep-Sea Res. Part A* **36**, 1721-1733.

Lighthill, M. J. (1952). On the squirming motion of nearly spherical deformable bodies through liquids at very small Reynolds numbers. *Comm. Pure Appl. Math.* **5**, 109-118.

MacKenzie, B. R., Miller, T. J., Cyr, S. and Leggett, W. C. (1994). Evidence for a dome-shaped relationship between turbulence and larval fish ingestion rates. *Limnol. Oceanogr.* **39**, 1790-1799.

Manahan, D. T. (1983). The uptake and metabolism of dissolved amino acids by bivalve larvae. *Biol. Bull.* **164**, 236-250.

Manahan, D. T. (1990). Adaptations by invertebrate larvae for nutrient acquisition from seawater. *Am. Zool.* **30**, 147-160.

Marrasé, C., Costello, J. H., Granata, T. and Strickler, J. R. (1990). Grazing in a turbulent environment: Energy dissipation, encounter rates, and efficacy of feeding currents in *Centropages hamatus*. *Proc. Natl. Acad. Sci.* **87**, 1653-1657.

Marsh, A. G. and Manahan, D. T. (1999). A method for accurate measurements of the respiration rates of marine invertebrate embryos and larvae. *Mar. Ecol. Progr. Ser.* **184**, 1-10.

Journal of Experimental Biology

Marsh, A. G., Leong, P. K. K. and Manahan, D. T. (1999). Energy metabolism during embryonic development and larval growth of an antarctic sea urchin. *J. Exp. Biol.* **202**, 2041-2050.
Maxey, M. R. and Riley, J. J. (1983). Equation of motion for a small rigid sphere in a nonuniform flow. *Phys. Fluids* **26**, 883-889.
McDonald, K. A. (2012). Earliest ciliary swimming effects vertical transport of planktonic embryos in turbulence and shear flow. *J. Exp. Biol.* **215**, 141-151.
Mei, R., Adrian, R. J. and Hanratty, T. J. (1991). Particle dispersion in isotropic turbulence under Stokes drag and Basset force with gravitational settling. *J. Fluid Mech.* **225**, 481-495.
Morris, M. J., Gust, G. and Torres, J. J. (1985). Propulsion efficiency and cost of transport for copepods: a hydromechanical model of crustacean swimming. *Mar. Biol.* **86**, 283-295.
Osterman, N. and Vilfan, A. (2011). Finding the ciliary beating pattern with optimal efficiency. *Proc. Natl. Acad. Sci.* **108**, 15727-15732.
Paffenhöfer, G.-A. (1971). Grazing and ingestion rates of nauplii, copepodids and adults of the marine planktonic copepod *Calanus helgolandicus*. *Mar. Biol.* **11**, 286-298.
Pan, T.-C. F., Applebaum, S. L. and Manahan, D. T. (2015). Experimental ocean acidification alters the allocation of metabolic energy. *Proc. Natl. Acad. Sci.* **112**, 4696-4701.
Pechenik, J. A. (2006). Larval experience and latent effects – metamorphosis is not a new beginning. *Integr. Comp. Biol.* **46**, 323-333.
Pepper, R. E., Jaffe, J. S., Variano, E. and Koehl, M. A. R. (2015). Zooplankton in flowing water near benthic communities encounter rapidly fluctuating velocity gradients and accelerations. *Mar. Biol.* **162**, 1939-1954.
Phillips, N. E. (2002). Effects of nutrition-mediated larval condition on juvenile performance in a marine mussel. *Ecology* **83**, 2562-2574.
Pörtner, H. O., Dupont, S., Melzner, F., Storch, D. and Thorndyke, M. (2010). Studies of metabolic rate and other characteristics across life stages. In *Guide to Best Practices for Ocean Acidification Research and Data Reporting* (ed. U. Riebesell, V. J. Fabry, L. Hansson and J.-P. Gattuso), pp. 167-180. Luxembourg: Publications Office of the European Union.
Reinfelder, J. R. and Fisher, N. S. (1994). The assimilation of elements ingested by marine planktonic bivalve larvae. *Limnol. Oceanogr.* **39**, 12-20.
Rothschild, B. J. and Osborn, T. R. (1988). Small-scale turbulence and plankton contact rates. *J. Plankton Res.* **10**, 465-474.
Rubey, W. W. (1933). Settling velocity of gravel, sand, and silt particles. *Am. J. Sci.* **25**, 325-338.
Saiz, E. and Kiørboe, T. (1995). Predatory and suspension feeding of the copepod *Acartia tonsa* in turbulent environments. *Mar. Ecol. Prog. Ser.* **122**, 147-158.
Saiz, E., Calbet, A. and Broglio, E. (2003). Effects of small-scale turbulence on copepods: The case of *Oithona davisae*. *Limnol. Oceanogr.* **48**, 1304-1311.
Shilling, F. M. and Manahan, D. T. (1994). Energy metabolism and amino acid transport during early development of Antarctic and temperate echinoderms. *Biol. Bull.* **187**, 398-407.
Shimeta, J. and Jumars, P. A. (1991). Physical mechanisms and rates of particle capture by suspension-feeders. *Oceanogr. Mar. Biol. Annu. Rev.* **29**, 191-257.
Shy, S. S., Tang, C. Y. and Fann, S. Y. (1997). A nearly isotropic turbulence generated by a pair of vibrating grids. *Exp. Therm. Fluid Sci.* **14**, 251-262.
Sleigh, M. A. and Blake, J. R. (1977). Methods of ciliary propulsion and their size limitations. In *Scale Effects in Animal Locomotion* (ed. T. J. Pedley), pp. 243-256. London: Academic Press.
Strathmann, R. R. (1975). Larval feeding in echinoderms. *Amer. Zool.* **15**, 717-730.
Strathmann, R. R. and Leise, E. (1979). On feeding mechanisms and clearance rates of molluscan veligers. *Biol. Bull.* **157**, 524-535.
Stumpp, M., Wren, J., Melzner, F., Thorndyke, M. C. and Dupont, S. T. (2011). CO_2 induced seawater acidification impacts sea urchin larval development I: Elevated metabolic rates decrease scope for growth and induce developmental delay. *Comp. Biochem. Physiol. A* **160**, 331-340.
Styles, R. (2015). Flow and turbulence over an oyster reef. *J. Coastal Res.* **31**, 978-985.
Sutherland, K. R., Costello, J. H., Colin, S. P. and Dabiri, J. O. (2014). Ambient fluid motions influence swimming and feeding by the ctenophore *Mnemiopsis leidyi*. *J. Plankton Res.* **36**, 1310-1322.
Taylor, G. I. (1935). Statistical theory of turbulence. *Proc. R. Soc. Lond. A* **151**, 421-444.
Thorson, G. (1950). Reproductive and larval ecology of marine bottom invertebrates. *Biol. Rev.* **25**, 1-45.
Tucker, V. A. (1975). The energetic cost of moving about: Walking and running are extremely inefficient forms of locomotion. Much greater efficiency is achieved by birds, fish - and bicyclists. *Am. Sci.* **63**, 413-419.
Variano, E. A. and Cowen, E. A. (2008). A random-jet-stirred turbulence tank. *J. Fluid Mech.* **604**, 1-32.
Visser, A. W., Mariani, P. and Pigolotti, S. (2009). Swimming in turbulence: zooplankton fitness in terms of foraging efficiency and predation risk. *J. Plankton Res.* **31**, 121-133.
Warkentin, M., Freese, H. M., Karsten, U. and Schumann, R. (2007). New and fast method to quantify respiration rates of bacterial and plankton communities in freshwater ecosystems by using optical oxygen sensor spots. *Appl. Environ. Microbiol.* **73**, 6722-6729.
Webster, D. R., Brathwaite, A. and Yen, J. (2004). A novel laboratory apparatus for simulating isotropic oceanic turbulence at low Reynolds number. *Limnol. Oceanogr. Methods* **2**, 1-12.
Webster, D. R., Young, D. L. and Yen, J. (2015). Copepods' response to Burgers' vortex: deconstructing interactions of copepods with turbulence. *Integr. Comp. Biol.* **55**, 706-718.
Wheeler, J. D., Helfrich, K. R., Anderson, E. J., McGann, B., Staats, P., Wargula, A. E., Wilt, K. and Mullineaux, L. S. (2013). Upward swimming of competent oyster larvae *Crassostrea virginica* persists in highly turbulent flow as detected by PIV flow subtraction. *Mar. Ecol. Prog. Ser.* **488**, 171-185.
Whitehill, E. A. G. and Moran, A. L. (2012). Comparative larval energetics of an ophiuroid and an echinoid echinoderm. *Invert. Biol.* **131**, 345-354.
Wilkin, J. L. and Jeffs, A. G. (2011). Energetics of swimming to shore in the puerulus stage of a spiny lobster: can a postlarval lobster afford the cost of crossing the continental shelf? *Limnol. Oceanogr. Fluids Environ.* **1**, 163-175.
Zeuthen, E. (1953). Oxygen uptake as related to body size in organisms. *Q. Rev. Biol.* **28**, 1-12.